Highly Anisotropic Elements for Acoustic Pentamode Applications

Christopher N. Layman* and Christina J. Naify
National Research Council, Washington, DC 20001, USA

Theodore P. Martin, David C. Calvo, and Gregory J. Orris
U.S. Naval Research Laboratory, Washington, DC 20375, USA

(Received 20 November 2012; revised manuscript received 22 April 2013; published 10 July 2013)

Pentamode metamaterials are a class of acoustic metafluids that are characterized by a divergence free modified stress tensor. Such materials have an unconventional anisotropic stiffness and isotropic mass density, which allow themselves to mimic other fluid domains. Here we present a pentamode design formed by an oblique honeycomb lattice and producing customizable anisotropic properties. It is shown that anisotropy in the stiffness can exceed 3 orders of magnitude, and that it can be realistically tailored for transformation acoustic applications.

DOI: 10.1103/PhysRevLett.111.024302 PACS numbers: 43.40.+s, 62.30.+d, 81.05.Xj

Introduction.—Metamaterials comprise a relatively new area of research, which utilizes a wave-functionalized microstructure to yield unconventional effective material properties. With its origin in microwave optics [1], domains of study have since expanded to include near-infrared and visible optics [2,3], radio-frequency electronics [4], and magnetics [5].

Many of the exotic phenomena observed in optical metamaterials, such as negative refraction and near-zero permittivity, have inspired analogous studies in acoustics [6–9] and elastodynamics [10,11]. Additionally, coordinate transformation methods [12] have generated new acoustic device concepts that do not require material negativity, such as lenses [13], beam splitters [14], black holes [15], and scattering reducing cloaks [16–19]. Such devices are defined as metafluids, which are effective materials with unconventional fluid-like properties whose particular bulk realization typically requires an anisotropic mass density. Experimental demonstration has been sparse, with most studies relying on a superlattice approach of alternating isotropic layers [20]. However, such an approach is difficult to realize and limited by the so-called mass catastrophe, which requires infinite mass density in the effective material profile.

An alternative approach is to generalize the conventional stress strain relationship to include pentamode metamaterials. Pentamode materials [21–23] are metafluids that support five easy infinitesimal strains (i.e., there is only one nonzero eigenvalue of the elasticity tensor which is of a pure pressure type), and satisfies the invariance of the governing equations by virtue of maintaining a harmonic transformation. Pure pentamodes, in general, have an isotropic density and anisotropic stiffness with a negligible shear modulus. Recently, a fabricated isotropic pentamode material was shown to have an effective bulk modulus to shear modulus ratio that potentially exceeds 3 orders of magnitude [24]. However, it has yet to be reported that anisotropic pentamode metamaterials can be realistically implemented for specific applications, since an elastic solid with a zero shear modulus would have no stability and immediately flow away.

In this Letter, we show that an oblique honeycomb lattice can be utilized as a simple yet versatile building block for pentamode device construction, which exerts highly anisotropic control over sound waves. The method presents a distinctly different approach to acoustic metamaterials, in that it does not require the difficult to achieve high value anisotropy in the effective mass density in addition to removing frequency bandwidth problems associated with inertial metafluids. Potential applications include extraordinary scattering reduction and arbitrary wave manipulation, low loss acoustic delay lines [25], and phase controlled logic gates [26].

Anisotropy in pentamode metafluids.—We consider elastic wave propagation in a microstructure having the general characteristics presented in Fig. 1. For simplicity we present our results in a two-dimensional (2D) plain strain space; however, the analysis can straightforwardly be extended to three dimensions. Only wavelengths much larger than the lattice constants $\mathbf{a}_1$ and $\mathbf{a}_2$ are considered to achieve a homogeneous approximation. As shown in Fig. 1 the strut angle β can be tuned to create isotropic ($\beta \sim 30°$), highly anisotropic ($\beta \sim 0°$), and reentrant ($\beta < 0°$) materials. Hence, based upon a targeted property profile, a gradient structure can be designed having smoothly varying properties related to the local changing microstructure. The condition that $\mathbf{a}_1$ remain constant throughout does not effect the generality of the results presented.

To demonstrate the properties of the structure, finite element analysis (COMSOL MULTIPHYSICS) was used to determine the structural eigenfrequenies of each geometric permutation, which has Bloch-Floquet periodic conditions prescribed on the unit cell boundaries. This is analogous to

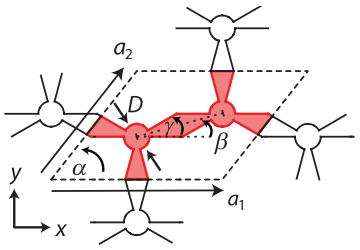

FIG. 1 (color). Schematic of an anisotropic 2D pentamode microstructure, with one unit cell highlighted. Bulk effective properties were tuned with variation in cell geometry including joint diameter D, strut angle β, and inner-strut angle γ. The unit cell angle α is obtained by $\alpha = \tan^{-1}[1 + \tan(\beta)]$, with $-15° < \beta < 30°$. $\mathbf{a}_1$ is held fixed throughout.

computing the elastic wave band structure where the first two eigenfrequencies correspond to quasishear (qS) and quasilongitudinal (qL) modes, respectively (see below for discussion on quasimodes). These two eigenfrequencies were selected at small values of the wave number, near the origin where the dispersion curves are linear, to obtain long wavelength quasishear v_{qS} and quasilongitudinal v_{qL} phase speeds. An anisotropy factor ξ is then defined as the ratio of effective bulk modulus in the principle directions,

$$\xi = \frac{K_x}{K_y} = \frac{[v_{\mathrm{qL}}^2 - v_{\mathrm{qS}}^2]_x}{[v_{\mathrm{qL}}^2 - v_{\mathrm{qS}}^2]_y}. \tag{1}$$

Similarly, a pentamode factor Δ, which assesses the contribution of the shear, is defined as

$$\Delta_{x,y} = \left[\frac{v_{\mathrm{qL}}^2 - v_{\mathrm{qS}}^2}{v_{\mathrm{qL}}^2}\right]_{x,y}, \tag{2}$$

where the subscript represents the propagation direction. In the above equations it is assumed that the effective dynamic mass density $\tilde{\rho}$ is isotropic and equal to the volume averaged mass density [and hence is removed from Eqs. (1) and (2)]. Justification for this is shown in the Supplemental Material [27].

Figure 2(a) displays the calculated anisotropy factor, using the material properties of steel for the lattice and void for the interstitials, as a function of the geometric parameters β, γ, and $\bar{D}$, where $\bar{D} = D/|\mathbf{a}_1|$. Exponentially increasing anisotropy is seen as β approaches 0°, with ξ exceeding 10^3 for small γ and $\bar{D}$. Figures 2(b) and 2(c) display the calculated pentamode factor, for the same geometric conditions as in Fig. 2(a). When β is small, Δ itself can be anisotropic; the contribution to shear modes is negligible in the x direction [Fig. 2(b)] and substantial in the y direction [Fig. 2(c)]. This occurs because, in the weak direction, as β decreases towards 0 the compression modulus ($\sim v_{\mathrm{qL}}^2$) decreases faster than the shear modulus ($\sim v_{\mathrm{qS}}^2$).

In isotropic media, the displacement polarization of the propagating wave is either parallel or normal to the wave

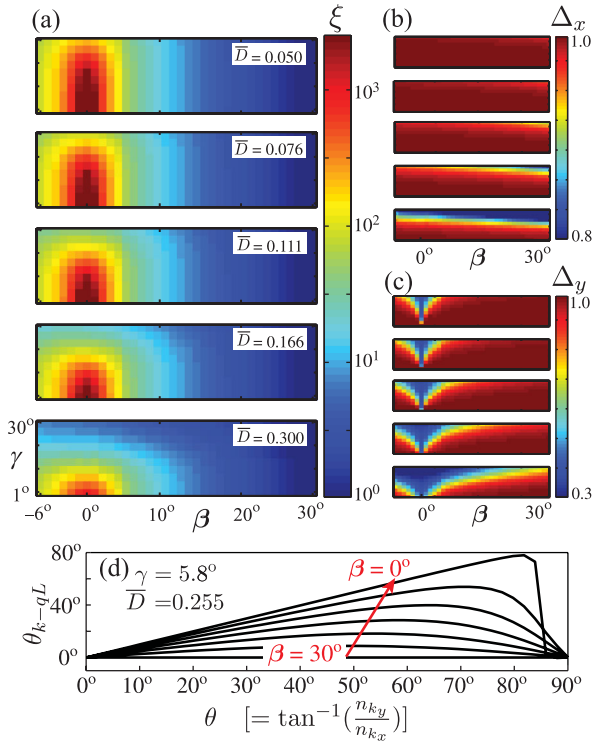

FIG. 2 (color). Properties of an anisotropic pentamode metafluid. (a) Anisotropy factor ξ as a function of unit cell geometric parameters, using the constituent properties of steel and lattice orientation as in Fig. 1. Pentamode factor Δ_x in the stiff direction (b) and Δ_y weak direction (c). Note scale difference between (b) and (c), and that the y axis in (b) and (c) is the same as in (a). (d) Behavior of quasimodes as the design becomes more anisotropic (small β) at high propagation angles (θ, which is measured from the horizontal axis). The volume fraction for the range of parameters covered in (a)–(d) spans from approximately 1.5% to 64%.

vector direction. In anisotropic media, however, this is in general not the case and waves propagate as quasilongitudinal (qL) and quasishear (qS) modes. The angle between the propagation direction $\mathbf{n}_k = \mathbf{k}/|\mathbf{k}|$ and the qL polarization direction $\mathbf{n}_{\mathrm{qL}}$ is expressed as

$$\theta_{k-\mathrm{qL}} = \cos^{-1}(\mathbf{n}_k \cdot \mathbf{n}_{\mathrm{qL}}). \tag{3}$$

Because qL and qS modes are orthogonal $\theta_{k-\mathrm{qS}} = \theta_{k-\mathrm{qL}} + \pi/2$, and for pure modes $\theta_{k-qL} = 0$. It is seen in Fig. 2(d) that under the current design there is a very strong dependence of $\theta_{k-\mathrm{qL}}$ on β, and that for small β there exists an extreme resistance of the wave to displace out of the stiff (x) direction. In summary, there are two phenomena that have the potential to affect material performance from the pentamode ideal, and both are born out of the relationship between the stiff (stretch-dominated) and weak (bending-dominated) directions of the lattice in the extreme anisotropic cases when β is small. One [Fig. 2(c)] involves an increasing role of the shear mode

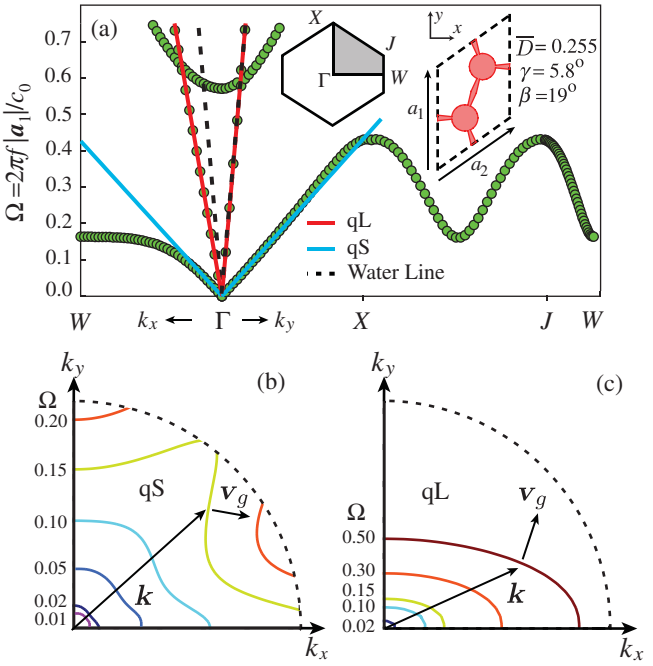

FIG. 3 (color). (a) Normalized band structure along the principal directions for the unit cell used in the acoustic mirage. Inset shows the unit cell and first Brillouin zone with the irreducible part shaded in gray. (b), (c) Equifrequency contours for qS and qL modes at selected frequencies (contours not calculated to zone boundaries). The dotted curve depicts the wave vector **k** direction, and anisotropic behavior is depicted by the difference between **k** and group velocity vector $\mathbf{v}_g$.

in the weak (y) direction due to a decreasing compression modulus, and the other [Fig. 2(d)] involves extreme deviation from pure propagating modes that tend to polarize along the stiff (x) direction for qL and weak (y) for qS.

Device applications.—To demonstrate the efficiency of our method to devise acoustic metafluids, we employ it to design two different transformation acoustic devices. The first one is based on the concept of an acoustic mirage, where an observer hears an echo from a distant wall, whereas in reality the echo originates from a much closer boundary. Norris [23] theoretically showed that a 2D mirage can be implemented using a pure pentamode metamaterial having orthotropic symmetry in the stiffness tensor. This metafluid, of length a, mimics a larger fluid domain, of length $a + d$, and is both impedance matched and has equivalent acoustic travel times, such that to an external observer the two domains are indistinguishable (see Fig. 4). The mirage density and bulk modulus are expressed as

$$\tilde{\rho} = \frac{a+d}{a}\rho_0, \qquad K = K_0\begin{bmatrix} \frac{a}{a+d} & 0 \\ 0 & \frac{a+d}{a} \end{bmatrix}, \tag{4}$$

where ρ_0 and K_0 are the density and bulk modulus of the background fluid, in the present case water. Using equation (4) the mirage device can now be designed by choosing a constituent material and adjusting the unit cell geometry to approximate the required properties.

Figure 3(a) shows the band structure of a unit cell [see inset of Fig. 3(a)] which approximately satisfies Eq. (4) for a mirage parameter of $a = d$, as a function of the normalized frequency $\Omega = 2\pi f|\mathbf{a}_1|/c_0$, where f is the circular frequency and c_0 is a reference sound speed (here water). For this choice of geometric parameters, $K_{11} = 0.5052K_0$, $K_{22} = 2.0K_0$, and $\tilde{\rho} = 2.037\rho_0$, as can be seen in the band structure. With using silver as the base material, $\xi = 0.24$, $\Delta_x = 0.96$, and $\Delta_y = 0.99$ (note that this cell is oriented differently as compared to Fig. 1). Other choices of base materials are possible, which would then require a new parameter search in an attempt to match Eq. (4). The device has a sufficient amount of shear for structural stability yet still retains pentamode characteristics. Additionally, a wideband shear-wave directional band gap is noticed for propagation in the weak (x) direction. Figures 3(b) and 3(c) show the equifrequency contours of the qS and qL modes at selected frequencies. At $\Omega < 0.01$ the qS modes are approximately isotropic, with deviation from circularity of less than 5%. For higher Ω the qS modes have both significant increasing anisotropy and dispersion, as indicated by the relationship between group velocity and wave vectors inside the lattice. The equifrequency contours for the qL mode, conversely, maintains

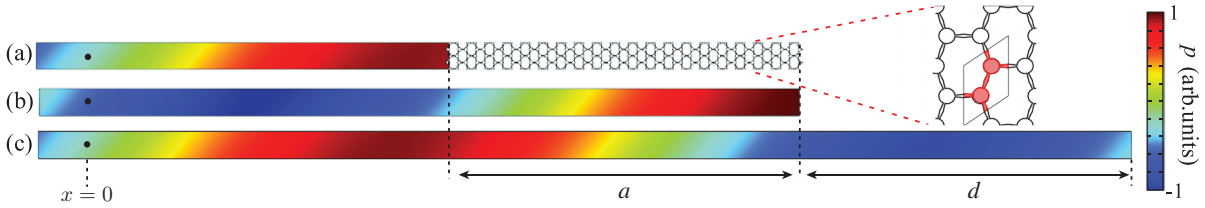

FIG. 4 (color). Acoustic mirage device for mirage parameter of $a = d$, showing the real part of the scattered pressure field, using water as the background fluid. Frequency $\Omega = 0.1$ and incident angle $\theta_i = 43.4°$; geometric parameters are those from Fig. 3. An observer at $x = 0$ sees the same acoustic field (amplitude and phase) with the pentamode metafluid (a) as without (c). For reference, a domain (b) is shown with the same length as the mirage. A plane wave travels from left to right, with imposed zero-reflection condition on left boundaries and zero normal displacement condition on right boundaries. Top and bottom boundaries have Bloch-Floquet conditions.

the required ellipsoidal anisotropy over a broad range of Ω. For a direct comparison between the fluid model of Eq. (4) and the unit cell properties see Supplemental Material Fig. 2 [27].

Using a unit cell with the specific properties obtained above, an acoustic mirage device is constructed as depicted in Fig. 4. Figures 4(a) and 4(c), respectively, compare the scattered acoustic fields for the mirage and the nonmirage case (the larger domain, termed the control), and they are seen to have excellent agreement. A reference domain is shown in Fig. 4(b). Since the pentamode design is not based on narrow resonances, the mirage will also operate over both a very wide frequency bandwidth and all angles of incidence. Figures 5(a) and 5(b) summarize the difference of the scattered pressure field amplitude δp and phase $\delta\phi$ between the mirage and control, with excellent agreement seen, though not perfect since there is a finite shear modulus in the lattice. This is compared to the reference, Figs. 5(c) and 5(d), which depend strongly on the incident angle and frequency between the two domains. See Supplemental Material [27] for additional discussion on mirage performance and sensitivity to design variables.

The above outlined method also has the flexibility to realize more complicated material profiles. To demonstrate this, we realize the material property values for a cylindrical pentamode scattering reduction layer for use in an aqueous environment. A graded anisotropic honeycomb lattice is used to simulate the transformed space, which reduces the actual size of the cylinder's radius a to virtual radius δ. One possible mapping function (though not unique) describing the transformation layer is [28]

$$f(r) = (b^2 - a^2)^{-1}\left[(b^2 - a\delta)r - (a - \delta)b^2\frac{a}{r}\right], \quad (5)$$

where r and b are the radial coordinate and outer radius of the transformation layer, respectively. Equation (5) maintains both radial impedance and orthogonal wave speed matching with the external fluid. Figure 6 compares the ideal pentamode material properties and values obtained from the composite metafluid for the case of $\delta = a/3$ and $b = 2a$, using steel as the base material. In 2D, pure pentamode properties can be obtained through [22]

$$\bar{K}_{\parallel}(r) = \frac{1}{f'(r)}\frac{f(r)}{r}, \qquad \bar{K}_{\perp}(r) = f'(r)\frac{r}{f(r)},$$
$$\bar{\rho}(r) = f'(r)\frac{f(r)}{r}, \qquad a \le r \le b, \quad (6)$$

where the overline represents normalization to water. Excellent agreement is demonstrated. For all cases of the designed properties, pentamode behavior is achieved, $\Delta_x = \Delta_y \sim 1$. At $r = a$, in Fig. 6, $\bar{K}_{\parallel} = 0.16$, $\bar{K}_{\perp} = 6.33$, and $\bar{\rho} = 0.70$. An inertial metafluid version of the transformation layer using Eq. (5) produces (at $r = a$) $\bar{K} = 1.42$, $\bar{\rho}_{\perp} = 0.157$, and $\bar{\rho}_{\parallel} = 6.33$. Using a superlattice approach to realize these inertial values requires alternating isotropic layers with properties $\bar{\rho}_1 = 12.58$, $\bar{K}_1 = 6.29$ and $\bar{\rho}_2 = 0.079$, $\bar{K}_2 = 0.80$. Realizing such a composite material is prohibitively difficult.

It is noted that Eq. (6) is for a cylindrical coordinate system, whereas the unit cell analysis is rectilinear. However, although it is the point of this work to demonstrate the feasibility to approximate unique property values required in pentamode applications, the design of a gradient curved structure based upon an anisotropic honeycomb lattice is beyond the scope of the current work and will be presented elsewhere. Furthermore, since the method is fully scalable, the local difference between the two systems decreases with decreasing unit cell size.

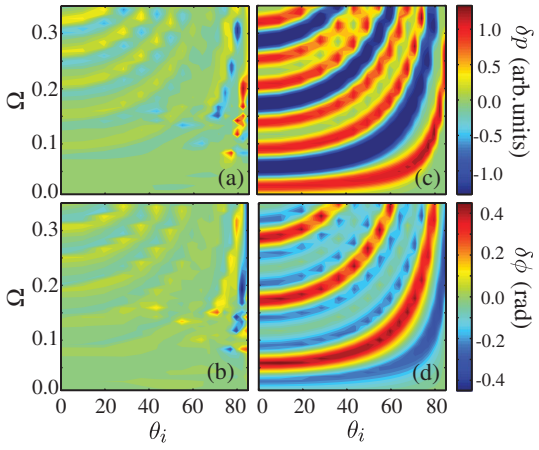

FIG. 5 (color). Difference of scattered pressure amplitude (δp) and phase ($\delta\phi$) of the mirage (a) and (b), and reference domain (c) and (d), evaluated at a point location far from the water-metafluid interface, $x = 0$. Plotted as a function of normalized frequency Ω and incident angle θ_i.

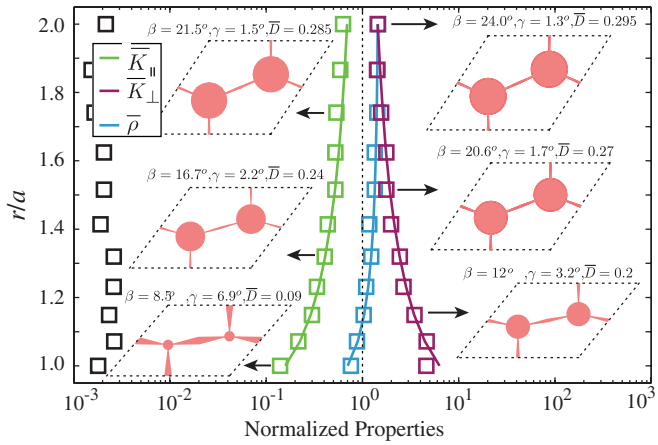

FIG. 6 (color). Material properties for transformation acoustics scattering reduction. Solid lines denote ideal fluid pentamode properties and symbols are properties achieved under the current design. Black squares denote shear modulus normalized to K_0.

See Supplemental Material [27] for further discussion on the scattering performance of a pentamode scattering reduction layer, based on a system of homogenized layers with properties obtained (including shear) from the method described above. We lastly note a concurrent work [29], which also explored anisotropy in pentamode systems.

Conclusions.—A versatile method to design and characterize highly anisotropic pentamode elements for transformation acoustics was presented. The design method is based upon customizing the geometric parameters of an oblique honeycomb lattice to target particular transformation acoustics applications. In the low frequency limit, the metallic structures act as acoustic metafluids with pentamode properties, and have negligible shear modulus relative to its anisotropic fluidlike stiffness. The simplicity of the design (easy to fabricate) coupled with the effectiveness of performance shows promise to realize concepts hitherto constrained by inertial-based metamaterial constructions.

This work was supported by the Office of Naval Research. We acknowledge useful discussions with Andy Norris, Jeff Cipolla, and Nachiket Gokhale.

*christopher.layman.ctr@nrl.navy.mil

[1] R. A. Shelby, D. R. Smith, and S. Schultz, Science **292**, 77 (2001).
[2] S. Zhang, W. Fan, K. J. Malloy, S. Brueck, N. C. Panoiu, and R. M. Osgood, Opt. Express **13**, 4922 (2005).
[3] G. Dolling, M. Wegener, C. M. Soukoulis, and S. Linden, Opt. Lett. **32**, 53 (2007).
[4] B. Edwards and N. Engheta, Phys. Rev. Lett. **108**, 193902 (2012).
[5] Y. Kobljanskyj, G. Melkov, K. Guslienko, V. Novosad, S. D. Bader, M. Kostylev, and A. Slavin, Sci. Rep. **2** 478 (2012).
[6] J. Li and C. T. Chan, Phys. Rev. E **70**, 055602 (2004).
[7] Y. Ding, Z. Liu, C. Qiu, and J. Shi, Phys. Rev. Lett. **99**, 093904 (2007).
[8] A. Sukhovich, L. Jing, and J. H. Page, Phys. Rev. B **77**, 014301 (2008).
[9] Y. Wu, Y. Lai, and Z.-Q. Zhang, Phys. Rev. Lett. **107**, 105506 (2011).
[10] M. K. Lee, P. S. Ma, I. K. Lee, H. W. Kim, and Y. Y. Kim, Appl. Phys. Lett. **98**, 011909 (2011).
[11] J. Christensen and F. J. G. de Abajo, Phys. Rev. Lett. **108**, 124301 (2012).
[12] H. Chen and C. T. Chan, J. Phys. D **43**, 113001 (2010).
[13] C. N. Layman, T. P. Martin, K. M. Moore, D. C. Calvo, and G. J. Orris, Appl. Phys. Lett. **99**, 163503 (2011).
[14] J. Bucay, E. Roussel, J. O. Vasseur, P. A. Deymier, A.-C. Hladky-Hennion, Y. Pennec, K. Muralidharan, B. Djafari-Rouhani, and B. Dubus, Phys. Rev. B **79**, 214305 (2009).
[15] Z. Chang and G. Hu, Appl. Phys. Lett. **101**, 054102 (2012).
[16] H. Chen and C. T. Chan, Appl. Phys. Lett. **91**, 183518 (2007).
[17] B.-I. Popa and S. A. Cummer, Phys. Rev. B **83**, 224304 (2011).
[18] N. Stenger, M. Wilhelm, and M. Wegener, Phys. Rev. Lett. **108**, 014301 (2012).
[19] B.-I. Popa, L. Zigoneanu, and S. A. Cummer, Phys. Rev. Lett. **106**, 253901 (2011).
[20] D. Torrent and J. Sanchez-Dehesa, Phys. Rev. Lett. **105**, 174301 (2010).
[21] G. Milton, *The Theory of Composites* (Cambridge University Press, Caimbridge, England, 2002).
[22] A. N. Norris, Proc. R. Soc. A **464**, 2411 (2008).
[23] A. N. Norris, J. Acoust. Soc. Am. **125**, 839 (2009).
[24] M. Kadic, T. Buckmann, N. Stenger, M. Thiel, and M. Wegener, Appl. Phys. Lett. **100**, 191901 (2012).
[25] R.-C. Yin, S.-Y. Yu, C. He, M.-H. Lu, and Y.-F. Chen, Appl. Phys. Lett. **97**, 092905 (2010).
[26] S. Bringuier, N. Swinteck, J. O. Vasseur, J.-F. Robillard, K. Runge, K. Muralidharan, and P. A. Deymier, J. Acoust. Soc. Am. **130**, 1919 (2011).
[27] See Supplemental Material at http://link.aps.org/supplemental/10.1103/PhysRevLett.111.024302 for additional analysis of the acoustic response of pentamode materials, including the scatter reduction performance.
[28] N. H. Gokhale, J. L. Cipolla, and A. N. Norris, J. Acoust. Soc. Am. **132**, 2932 (2012).
[29] M. Kadic, T. Bückmann, R. Schittny, and M. Wegener, New J. Phys. **15**, 023029 (2013).